Research Square

Preprints are preliminary reports that have not undergone peer review.
They should not be considered conclusive, used to inform clinical practice,
or referenced by the media as validated information.

Asymmetric risks of severe convective storms to US Agriculture

Zhe Zhang

zhezhang@ucar.edu

NSF National Center for Atmospheric Research https://orcid.org/0000-0003-3771-240X

Cenlin He

National Center for Atmospheric Research https://orcid.org/0000-0002-7367-2815

Changhai Liu

National Center for Atmospheric Research (NCAR)

Yan Jiang

University of California, San Diego https://orcid.org/0000-0002-1472-2288

Jennifer Burney

Stanford University

James Done

https://orcid.org/0000-0002-1007-835X

Julia Kukulies

University of Reading

Erin Dougherty

NSF National Center for Atmospheric Research

Lulin Xue

National Center for Atmospheric Research

Liping Di

George Mason University

Article

Keywords:

Posted Date: November 26th, 2026

DOI: https://doi.org/10.21203/rs.3.rs-11059625/v1

License: This work is licensed under a Creative Commons Attribution 4.0 International License.
Read Full License

Additional Declarations: There is **NO** Competing Interest.

Title: Asymmetric risks of severe convective storms to US Agriculture

Author Information

Zhe Zhang[1*], Cenlin He[1*], Changhai Liu[1], Yan Jiang[2,3], Jennifer Burney[3], James M. Done[1], Julia Kukulies[1], Erin Dougherty[1], Lulin Xue[1], Liping Di[4]

Affiliations

[1] NSF National Center for Atmospheric Research, Boulder, CO, 80301, USA

[2] University of California, School of Global Policy and Strategy, San Diego, CA, 92093, USA

[3] Stanford University, Doerr School of Sustainability, Stanford, CA, 94305, USA

[4] George Mason University, Center for Spatial Information Science and Systems, Fairfax, VA, 22030, USA

Contributions

Z.Z., C.H., C.L., Y.J. and J.B conceptualized and designed the research. C.H. and Z.Z. conducted the model simulations and analysis. C.H., C.L., J.K., E.D., Y.J., J.D., J.B., L.X., and L.D. provided valuable discussions and advice. Z. Z., C.H., L.D., and L.X. obtained the funding. Z.Z. drafted the first version manuscript with help from C.H. All co-authors contributed to reviewing and improving the manuscript.

Corresponding author

Correspondence to: Zhe Zhang (zhezhang@ucar.edu), Cenlin He (cenlinhe@ucar.edu)

Abstract

Severe convective storms (SCS), including hails, tornadoes, and thunderstorm winds, drive multi-billion-dollar losses to US agriculture annually. However, the interplay between SCS hazards, cropland exposures, and agricultural vulnerability is complex, making understanding future impacts in a warming world difficult. Here, we address this gap by integrating severe weather reports, USDA crop insurance records, and high-resolution convection-permitting climate simulations to first understand the structure of US agricultural SCS risk; we then project its future changes under climate warming. We reveal an important asymmetry in the current risk structure in the central US "SCS Alley". In the Northern Great Plains and Corn Belt, SCS losses are primarily exposure-driven due to high agricultural liability, yet producers elect high coverage levels, effectively buffering them against adverse hazards. Conversely, along the southern periphery (the Southern Great Plains and Lower Mississippi Valley), losses are driven by higher physical hazard and vulnerability, yet producers carry lower coverage, thus absorbing disproportionately greater direct losses. Crucially, high-resolution climate projections indicate future increases in SCS will concentrate precisely on the under-prepared southern periphery, driving an estimated 11% increase in crop insurance indemnities, while the highly insured northern part remains relatively stable (±3%). By explicitly linking physical hazards with crop insurance records, our work uncovers hidden structural vulnerabilities in the federal crop insurance program and provides actionable guidance for developing climate-resilient agricultural risk management and adaptation strategies.

Introduction

Severe convective storms (SCS), encompassing hailstorms, tornadoes, and damaging thunderstorm winds, rank among the most destructive natural hazards in the US, causing billions of dollars in annual losses across both the built and agricultural landscape (1-2). Specific to the agricultural sector, these losses concentrate in the spring and summer growing season, striking crops at their most vulnerable stages and posing a persistent threat to production and farm income (3-7). Yet the impacts from SCS ultimately depend on more than the physical hazards: it is largely moderated by to the extent to which agricultural value lies in harm's way (exposure) and by how susceptible that value is to SCS damage (vulnerability) (8-11). Assessing SCS risk to agriculture therefore requires integrating hazard, exposure, and vulnerability (12), one that becomes both harder and more consequential under the large uncertainty of a changing climate (13-15).

Accurately quantifying SCS hazard itself has historically been difficult, because the observational records are short and inconsistent, and alternatively, the conventional coarse-resolution climate models inadequately represent the convective processes that produce severe storms. Ground-based reports from the NOAA Storm Prediction Center (SPC) (16-17) have long served as the standard observational dataset for mapping SCS over the US. However, because they rely on human observers and reporting practices have evolved over time, the resulting record is spatially biased toward populated areas and temporally inhomogeneous. Where direct observation falls short, climatological studies have commonly employed environmental proxies for SCS, such as combinations of convective available potential energy (CAPE) and vertical wind shear that favor severe convection (18-19). Such proxies are readily simulated by coarse-resolution general circulation models (GCMs), but favorable environments alone are insufficient to guarantee storm initiation. More fundamentally, because GCMs parameterize instead of explicitly resolve convective storms, projections of SCS frequency and intensity remain highly uncertain, and moreover, the empirical relationship between large-scale environments and storm occurrence may not remain stationary under a changing climate (13). By contrast, high-resolution convection-permitting climate models (CPCMs) offer a promising alternative (20-21): by explicitly resolving convection, they avoid uncertainties associated with convective parameterization and capture the mesoscale dynamics governing storm initiation and evolution that drive hazardous weather across the US (22-26). Nonetheless, most climate research has largely focused on projecting future SCS hazards (15, 27-29), whereas much less attention has been paid to how those hazards translate to sector-specific risks, particularly in agriculture and the broader agro-economy (14, 30-31).

In parallel, a large body of economic research has used crop insurance records to quantify the impacts of climate variability and severe weather on agricultural production and farm income. The US Department of Agriculture (USDA) Federal Crop Insurance Program (FCIP), the primary financial safety net for US producers, has provided detailed claim-level cause-of-loss records for understanding this relationship (30, 32-37). That literature, however, has concentrated overwhelmingly on drought, heat, and excess moisture, while largely overlooking SCS-specific damages. Unlike drought or heat stresses, which build over weeks to months, SCS strikes within hours, inflicting acute, spatially localized, catastrophic, and often irreversible damage to crops. Because the FCIP is heavily subsidized, these losses ultimately impose financial burdens on both

producers and on the federal government via subsidies. Any increase in SCS hazards can translate directly into higher indemnities, premiums, and federal outlays, raising important questions of who ultimately bears the cost of SCS and how crop insurance policies can be designed to be effective, efficient, and equitable. Quantifying SCS risk within the crop insurance system is therefore essential for assessing the climate change impacts on US agriculture.

Here, we integrate meteorological observations, crop insurance records, and convection-permitting climate simulations to quantify the SCS risk to US agriculture, over both the historical period and a projected warming scenario, using a hazard–exposure–vulnerability framework. First, we characterize SCS hazards by constructing a historical climatology of SCS days from a 40-year, 4-km convection-permitting climate reanalysis (C404) and evaluate it against NOAA storm reports. Future changes in SCS hazard are then assessed using a parallel Pseudo Global Warming (PGW) simulation, generated by dynamical downscaling large-ensemble global climate model projections under SSP3-7.0. Second, we quantify exposure by insured liability from the USDA FCIP crop insurance records, capturing where and how much agricultural value is at risk to SCS. Third, we combine SCS hazard with crop insurance indemnities to quantify per-storm losses, providing a measure of the realized financial vulnerability. We further decompose historical indemnities into three complementary components: hazard, exposure, and vulnerability, and provide a first-order projection of how future changes in SCS hazard translate into crop insurance indemnities. This framework positions SCS as both a meteorological and socioeconomic risk to US agriculture, providing actionable guidance for designing climate-adaptive agricultural policies.

Results

Severe Convective Storms Alley in the US

We first construct an SCS-day climatology (Fig. 1a-b) for the primary growing season (March-September; Methods) using both NOAA SPC severe weather reports and C404 dataset. C404 closely reproduces the observed spatial pattern of the observed SCS-day (Fig. 1b). Elevated SCS activities are concentrated in the Central US, east of the Rocky Mountains and west of the Mississippi River, forming a south-north corridor that extends from Texas to Montana through the Great Plains. We refer to this corridor as the "SCS Alley" (Fig.1a-b, black contour), reflecting the spatial co-occurrence of elevated hail, tornado, and damaging wind hazards that are markedly higher than elsewhere (see Fig. S1 for three types of SCS separately). Discrepancies between C404 and SPC-derived SCS days show a strong dependence on the county population, where C404 tends to underestimate SCS days in densely populated counties, consistent with the well-documented population bias in severe weather reports from populated areas (Fig.1c). Accordingly, major metropolitan areas, including Chicago, St. Louis, Phoenix, and Salt Lake City, appear as localized maxima in the SPC climatology (Fig. 1a) but not in C404 (Fig. 1b).

Temporally, C404 shows a modest upward trend in Central US SCS Alley over the past four decades (+0.16 days per decade, $p<0.05$). By contrast, the SPC record shows no significant long-term trend (-0.19 days/decade, $p=0.367$), instead being dominated by an artificial discontinuity resulting from changes to the severe-hail reporting criterion and the subsequent filtering of redundant reports (Fig.1d; see also Methods). This discontinuity underscores the inhomogeneity of the SPC record and its limitation for long-term trend analysis, cautioning against incorporating non-stationary assumptions from a heterogeneous observational record into insurance underwriting and actuarial practice. Nevertheless, C404 shows strong agreement with the SPC data after the discontinuity point (2012-2020). The cumulative SCS days also agree closely between C404 and the SPC (Pearson's correlation R=1.00, Fig. 1e), demonstrating the capability of convection-permitting C404 reanalysis to accurately capture the crucial timing of SCS, particularly during the primary growing season (Fig. 1e).

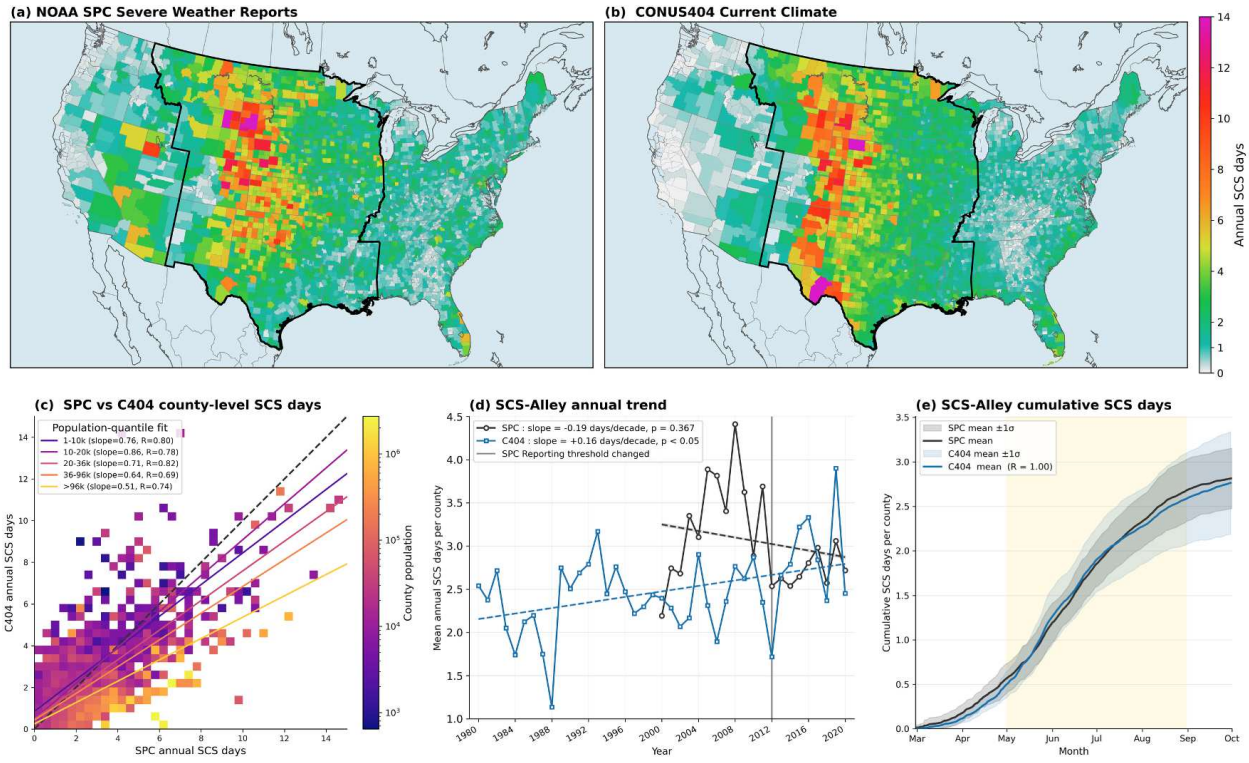


Fig.1. Spatial and temporal distribution of severe convective storms (SCS) in the United States during the primary growing season (March–September), based on NOAA SPC severe weather reports and C404 convection-permitting climate simulation. (a) County-level mean SCS days from NOAA SPC observations. (b) County-level mean SCS days from C404 current climate. The black state-level boundary outlines the Central US SCS Alley. (c) Scatter plot of county-level annual SCS days from NOAA SPC versus C404. Counties are colored by total population, the dashed line indicates the 1:1 reference and colored lines are quantile regression for different population quantiles, illustrating the systematic over-reporting in high-population counties in the SPC record. (d) Annual time series of mean SCS days within the SCS Hotspot from SPC (blue) and C404 (red, 1980–2020). The vertical line marks the 2011-2012 SPC reporting threshold change. Linear trends are shown as dashed lines. For more consistent comparison, (a-c) and (e) use the period of 2012-2020. (e) Intra-seasonal distribution of SCS days within the SCS Alley, shown as the cumulative distribution of the SCS days from Mar to Sep. Shaded bands indicate ±1 standard deviation. SPC mean (black), C404 mean (blue), and the shaded areas for ±1 σ are shown.

Exposure and Vulnerability to Severe Convective Storms

We quantify the exposure and vulnerability of the SCS impacts to US agriculture, using the USDA FCIP data. Because the FCIP subsidizes a large part of producer premiums on policies delivered by private insurers, enrollment approaches full coverage for major row crops, making insured liability a close proxy for the value of production at risk (38). As a baseline metric of exposure, we map the total FCIP insured liability for 2020 from the USDA Risk Management Agency (RMA) Summary of Business (SOB) and Cause of Loss (COL) (Fig. 2a and see Fig. S3 for insured liability and Fig. S4 for participation rate for five major crops). Cumulative national-level crop indemnities due to SCS total $USD 18.37 billion from 1989-2020 (Fig. 2b), ranking as the third-largest weather-related payments in the FCIP, after droughts and excessive moisture (30, see also Fig. S5). High SCS indemnities concentrate across a large swath of counties within the Central US SCS Alley (Fig. 1a), encompassing 18 states across the Corn Belt, the Great Plains, and the Lower Mississippi Valley (i.e., MT, WY, ND, SD, MN, IA, WI, IL, NE, CO, KS, MO, NM, TX, OK, AR, MS, LA; see Fig. S6 for state ranking of SCS indemnity). This pattern reflects the joint influence of frequent SCS (Fig. 1a-b) and large insured liabilities (Fig. 2a).

We next characterize two complementary metrics of vulnerability at county-level: crop insurance coverage level from SOB and aggregated per-storm loss (see Methods). Coverage level is an individual farmer choice shaped by federal policies and subsidy levels (as codified in the Farm Bill every 5+ years), regional historical practices, and perceived local risk (39-40). We treat coverage level as a vulnerability metric, for both farmers and taxpayers (and reinsurers), because it reflects how much risk is transferred to the FCIP versus absorbed by the producer. While the national median coverage level is 67%, coverage is markedly higher across the Corn Belt states (MN, WI, IA, NE, IL) and lower across several southern and interior-west states (NM, OK, TX, AR, LA, MS MT, WY) (Fig. 2c).

Per-storm loss is aggregated across growing seasons and crop types over the 1989-2020 claim history and is normalized by per $100 of insured liability. This normalized loss is similar to the loss-cost ratio (LCR, indemnity divided by liability), a commonly used measure in crop insurance research (7, 33-34, 37). Normalizing by $100 of exposure removes the effect of rising liability and inflation over the record, enabling direct comparisons across regions. Within the SCS Alley, per-storm loss is highest across the Great Plains and Interior West (TX, OK, KS, CO, WY, SD, ND, MT) and lower across the Corn Belt (Fig. 2d). This spatial pattern is consistent with the long-term crop-hail loss-cost record, in which loss costs have historically been highest in the Northern and Southern Plains and Mountain regions and the lowest in the Corn Belt (7, 41). We next examine the drivers of this geographical distribution, and its entanglement with coverage selection.

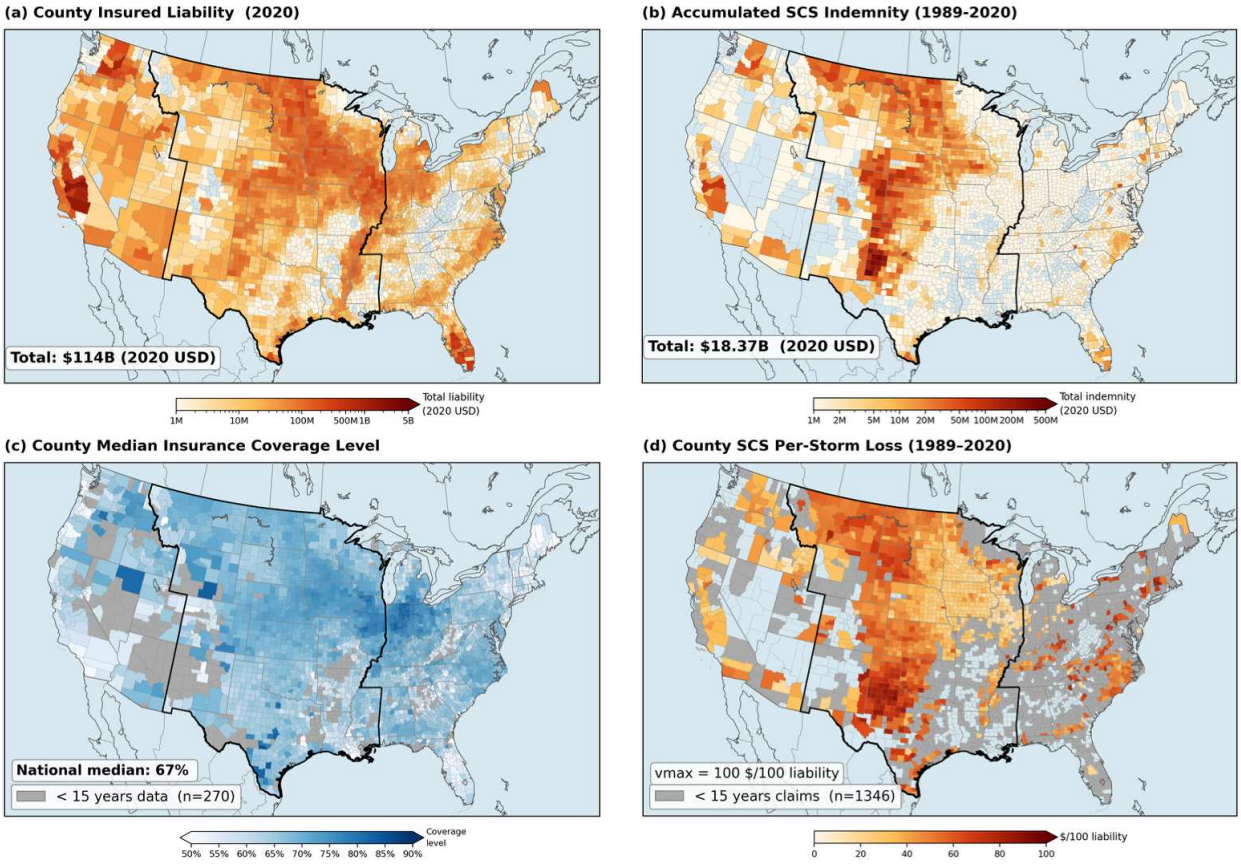


Fig. 2. National crop insurance liability, severe convective storm (SCS) indemnities, and financial vulnerability in the US FCIP. **(a)** County-level insured liability in 2020, (national total: $114B). **(b)** Cumulative FCIP indemnities attributed to SCS during 1989-2020, adjusted to USD2020 (totaling to $18.37B). **(c)** County-level median FCIP crop insurance coverage level, (national median: 67%). **(d)** County-level vulnerability to SCS, measured as per storm loss per 100 USD insured liability.

Attribution of Total Risk to Hazard, Exposure and Vulnerability

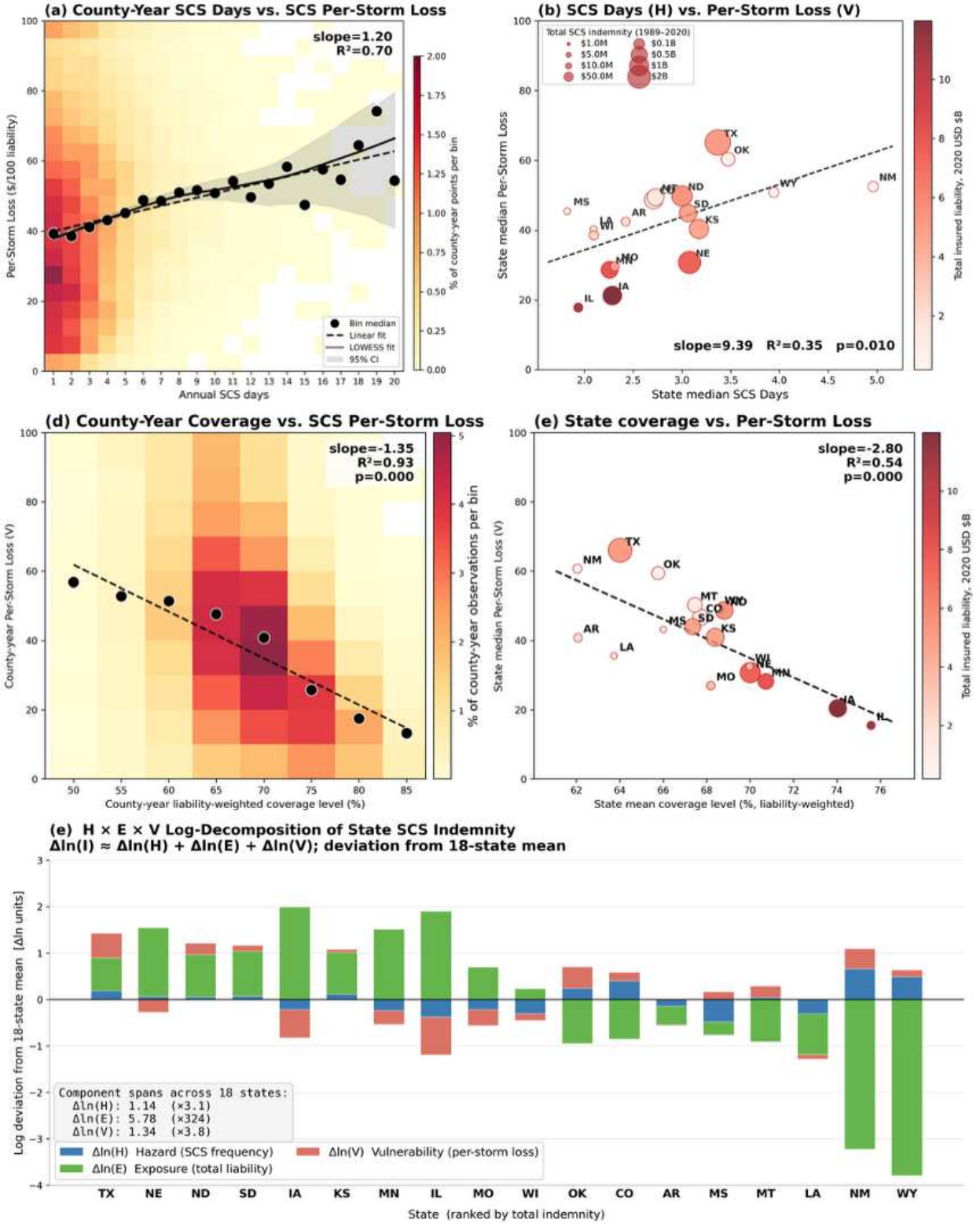
We characterize the hazard (SCS days, H), exposure (insured liability, E), and vulnerability (per-storm loss, V) across the 18 most SCS-impacted states in the SCS Alley and reveal an asymmetric structure that drives the largest differences in cumulative indemnity across states.

We first examine how per-storm loss covaries with SCS days at the county-year level (Fig. 3a, see Methods). The cross-sectional linear regression reveals a positive relationship, with per-storm loss increasing by 1.2 per additional SCS day (R=0.836), and narrow confidence intervals across the well-sampled range. Most claim data fall below six SCS days, with per-storm loss spanning 10-100 ($/100 liability). Data density reduces as SCS day rises (fewer claims); beyond 12 SCS days/year the record becomes sparse, leading to a sharp widening of the 95% confidence interval. Substantial heterogeneity exists across the claim data and SCS days within the 18-state SCS Alley. In states with rich data records (e.g., TX, NE, CO, MT), the linear relationship between SCS days and per-storm loss holds robustly, whereas states with fewer claims show vastly wider variability and correspondingly greater uncertainty in the fitted relationship, limiting confidence in extrapolating to high SCS day (see Fig. S7 and Table S1for state-level regressions). When aggregated to the state level and overlaying insured liability and total indemnity, a positive across-state relationship persists (Fig. 3b, slope=9.39, R=0.591, p=0.004). However, states with comparable SCS days can differ sharply in both per-storm loss and liability. For example, TX and NE, the top 2 states with the largest historical SCS losses, Texas exhibits a per-storm loss near 65 $/100 liability, more than twice that of Nebraska (30 $/100 liability).

What drives these substantial cross-state differences in per-storm loss? At both county-year level and across the 18 SCS Alley states, per-storm loss is negatively and significantly correlated with the elected coverage level (Fig. 3c-d). Coverage level is the yield-to-revenue fraction a producer elects to insure; it sets the deductible above which a loss becomes a claim, and thus how much risk is absorbed by the producer versus transferred to the FCIP. Where coverage is low, a storm whose yield impact stays above the coverage floor never generates a claim and is silent in the COL record; only the largest losses above the deductible are recorded. Higher-coverage regions (much of the Corn Belt) therefore record many more small claims, while lower-coverage regions (many southern states) record only severe events with higher loss (Fig. S8-S10). The elevated per-storm loss we observe in low-coverage states is thus, in large part, a structure of observable vulnerability rather than evidence that storms there are physically more damaging.

We further decompose each state's total indemnity into additive log-contributions from hazard, exposure, and vulnerability (Fig. 3e): $\Delta\ln(I) = \Delta\ln(H) + \Delta\ln(E) + \Delta\ln(V)$, expressed as deviations from the SCS Alley 18-state log-mean (zero line). This decomposition isolates the dominant drivers of total indemnity across states and quantifies how sensitive the total indemnity is to climatic and socio-economic components. Across the 18 SCS Alley states, exposure spans by far the widest range ($\Delta\ln(E)$=5.78, equivalent to 324-fold spread, versus 3.1-fold for hazard and 3.8-fold for vulnerability). Exposure is therefore the most variable and most decisive component in setting the differences of total SCS-indemnity across states. Texas ranks highest in total indemnity, exhibiting positive contributions across all three risk components, a pattern shared by North Dakota, South Dakota, and Kansas. By contrast, Nebraska ranks second almost entirely because

of exceptionally high exposure, where elevated liability offsets below-average vulnerability. Note that Nebraska straddles the rainfed-irrigated transition, thus drought and heat risk contribute additionally to high coverage levels and raise insured liability. The decomposition reveals a clear geographic asymmetry: Corn Belt states (NE, IA, IL, MN, MO) are characterized by above-average exposure with hazard and vulnerability remaining near or below average. Conversely, several lower-liability states (OK, CO, MT, NM, WY) have relatively modest insured liabilities despite experiencing above-average hazard and vulnerability.


(a) County-Year SCS Days vs. SCS Per-Storm Loss
slope=1.20
R²=0.70
Per-Storm Loss ($/100 liability)
Annual SCS days
% of county-year points per bin
Bin median
Linear fit
LOWESS fit
95% CI
(b) SCS Days (H) vs. Per-Storm Loss (V)
Total SCS indemnity (1989-2020)
$1.0M
$5.0M
$10.0M
$50.0M
$0.1B
$0.5B
$1B
$2B
State median Per-Storm Loss
State median SCS Days
Total insured liability, 2020 USD $B
slope=9.39 R²=0.35 p=0.010
(d) County-Year Coverage vs. SCS Per-Storm Loss
slope=-1.35
R²=0.93
p=0.000
County-year Per-Storm Loss (V)
County-year liability-weighted coverage level (%)
% of county-year observations per bin
(e) State coverage vs. Per-Storm Loss
slope=-2.80
R²=0.54
p=0.000
State median Per-Storm Loss (V)
State mean coverage level (%, liability-weighted)
Total insured liability, 2020 USD $B
(e) H × E × V Log-Decomposition of State SCS Indemnity
ΔIn(I) ≈ ΔIn(H) + ΔIn(E) + ΔIn(V); deviation from 18-state mean
Log deviation from 18-state mean [ΔIn units]
Component spans across 18 states:
ΔIn(H): 1.14 (×3.1)
ΔIn(E): 5.78 (×324)
ΔIn(V): 1.34 (×3.8)
ΔIn(H) Hazard (SCS frequency)
ΔIn(E) Exposure (total liability)
ΔIn(V) Vulnerability (per-storm loss)
TX NE ND SD IA KS MN IL MO WI OK CO AR MS MT LA NM WY
State (ranked by total indemnity)

228

Fig. 3. Hazard-Exposure-Vulnerability relationship underlying SCS-related indemnity across the Central US SCS Alley. **(a)** Cross-sectional linear regression between SCS days vs. per storm loss for the top 18 most-impacted states and 2D histogram for data density. **(b)** Cross-state scatter plot for the SCS days (x-axis), per storm loss (y-axis), insured liability (color) and total indemnity. Bubble size and color denote cumulative indemnity and insured liability, respectively. See Table S1 and Fig. S7 for the linear regression statistics for individual states. **(c)** Cross-sectional linear regression for coverage level and per-storm loss and 2D histogram for data density. **(d)** Cross state scatter for state-level coverage level vs. per storm loss. See Fig. S8-10 for the per-storm loss and coverage level distributions for individual states. **(e)** Decomposition of state-level total indemnity into log-contribution from hazard (blue), exposure (green), and vulnerability (red), expressed as deviations from the 18-state log mean (zero line). States are ordered left to right by total indemnity from highest to lowest. Positive (negative) values indicate above-average (below-average) contribution relative to the 18-state mean.

Future Severe Storm Risks Shift towards Historically Unprepared Regions

We project near-future changes in SCS hazard during 2022-2063 using the C404 parallel pseudo global warming (PGW) simulation under the SSP3-7.0 scenario and estimate the changes in crop insurance indemnities. The projection reveals two contrasting spatial patterns across the SCS Alley (Fig. 4a). In the northern part of the region (Northern Great Plains and Corn Belt), annual SCS days decline, driven predominantly by a summer (JJA) reduction that outweighs a slight spring (MAM) increase. In contrast, in the southern part (Southern Great Plains and Lower Mississippi), SCS days increase across both spring and summer, shifting the overall distribution towards more frequent storms (paired t-test significant in 22% of southern counties, versus 0% of northern counties; Fig. 4bc). To quantify the financial impact of this hazard shift, we propagate changes in SCS days into crop insurance indemnities using the multiplicative risk framework: $I = H \times E \times V$. Holding exposure (E, liability) and coverage level at their 2020 baseline isolate the projected indemnity changes to shifts in hazard (H) and per-storm loss (V). Future indemnity projection also shows an asymmetric growth in the southern states increasing by +11%, while the northern states show minimal change (±3%) (Fig. 4d-e; See Fig. S11 for seasonal projections in spring and summer).

This projected asymmetric shift in SCS indemnities towards higher losses in the southern states compound with its existing structural vulnerability of low coverage level, high per-storm loss, and sparse historical data in both SCS days and claims. Low coverage underpins these vulnerabilities by shifting a larger share of financial losses onto producers rather than the FCIP, while left-truncating the observable loss record, therefore inflating observed per-storm losses. Furthermore, in the Lower Mississippi (AR, MS, LA), historical SCS days have rarely exceeded 6 days per year. Future projections, however, extend beyond this historical range, implying that these regions may face increasing hazard under conditions for which historical observations provide a limited basis for estimating, pricing, and managing risk. Taken together, projected increases in SCS hazard fall asymmetrically on regions least prepared to price and absorb the associated risks, compounding increasing physical hazard with persistently low insurance coverage level. As a result, risk grows most rapidly where the insurance system has the weakest historical basis for assessing, pricing, and transferring that risk.

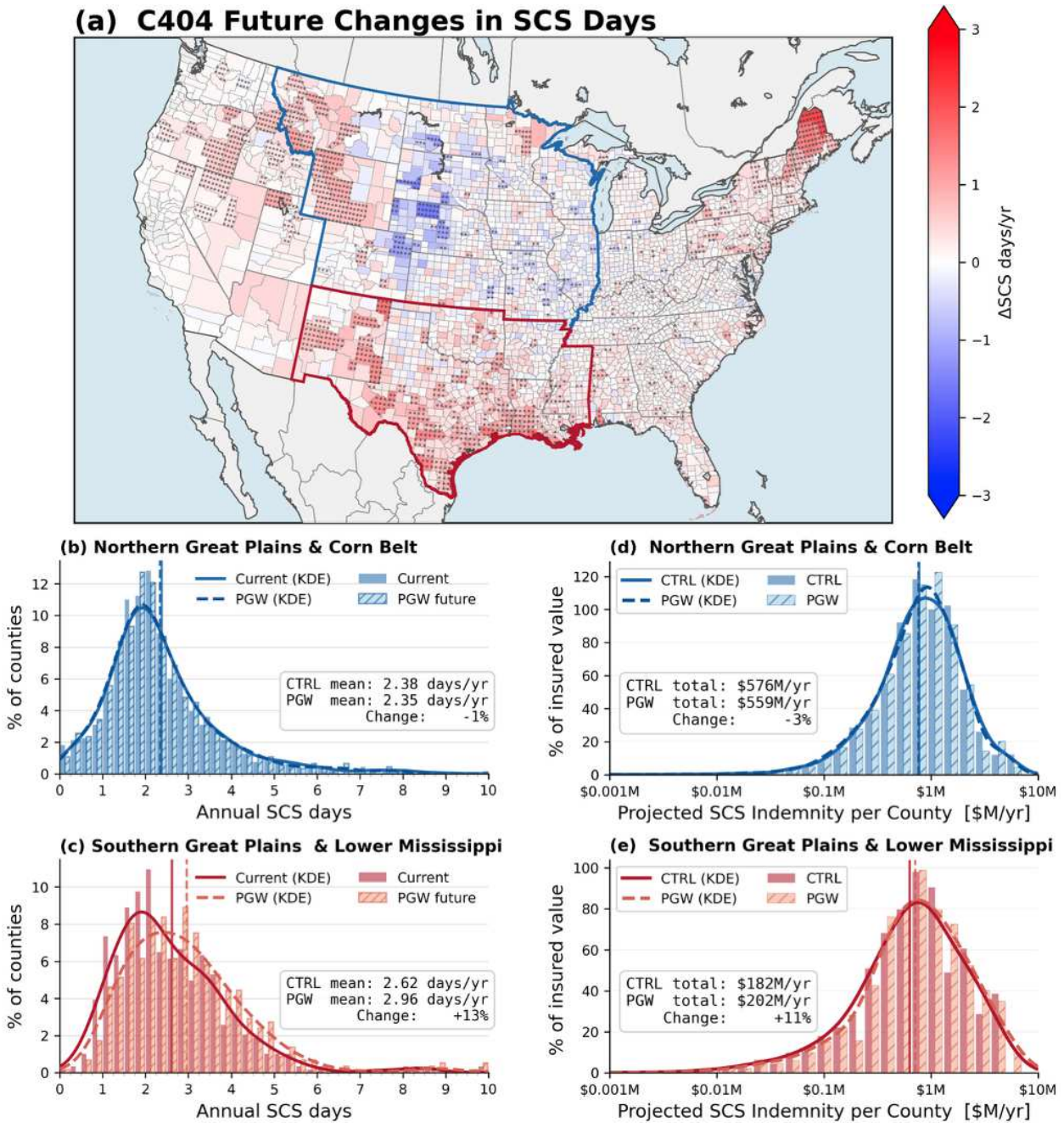


Fig. 4. Projected changes in SCS hazard and associated crop insurance indemnities. (a) Projected change in growing season SCS days during 2022-2063 from the C404 PGW simulation under the SSP3-7.0 scenario, relative to the historical baseline. The 18 most-impacted states separate into two contrasting regions: the Northern Great Plains and Corn Belt (NGP/CB) and Southern Great Plains and Lower Mississippi (SGP/LM). See Fig. S11 for future SCS days for spring and summer. (b, c) Historical and projected distribution of SCS days for the NGP/CB and SGP/LM; (d, e) Corresponding projected relative changes in SCS-related crop insurance indemnities.

Discussion and Implication

We investigated the risks posed by severe convective storms (SCS) to US agriculture by integrating three complementary datasets: NOAA SPC storm reports, high-resolution convection-permitting climate simulations (C404), and USDA crop insurance data. Although the projected change is modest when aggregated across the Central US SCS Alley, their geographical distribution shifts sharply and asymmetrically under climate change. Future SCS frequency increases most prominently across the Southern Great Plains (NM, TX, OK) and Lower Mississippi (AR, LA, MS), while slightly declining across the Northern Great Plains and Corn Belts. This spatial pattern translates into a first-order southern indemnity increase of 11% against a roughly flat north. Our central finding is that agricultural SCS risk is structurally asymmetric and intensifies under climate change, shifting physical hazards and their induced financial losses into regions of low preparedness and high vulnerability.

Physically, the future SCS hazard shifts are driven by a widespread, robust increase in the convective available potential energy (CAPE) across seasons that outweighs a modest decline in vertical wind shear. The overall thermodynamic tendency, characterized by elevated SCS potential in the Southern Great Plains, is broadly consistent with GCM projections (18-19), previous PGW downscaling under the RCP8.5 scenario (26), and more recent AI/ML downscaling efforts (42). This consensus across methodologies strengthens confidence in the projected spatial pattern of SCS risk. The projected summertime declines over the Northern Great Plains, however, is precisely an area where traditional environment-based proxies (e.g., CAPE–shear combinations) tend to diverge, because SCS response depends on the local balance between rising CAPE and weakening shear that coarse-resolution models cannot adequately represent. By contrast, convection-permitting resolution in C404 explicitly resolves the mesoscale processes that govern storm initiation rather than inferring storm occurrence from large-scale environments.

By linking physical climate hazards ("where will storms occur?") with socioeconomic risk ("where will storms cause the greatest damage?"), our study addresses a critical gap often overlooked in climate science and agroeconomic studies. The current SCS risk structure already anticipates which regions are most exposed to future changes. Decomposing each state's total indemnity into hazard, exposure, and vulnerability shows that some regions are effectively inelastic to SCS changes because their risk is exposure-driven. For example, the Corn Belt's dominant contribution is insured liability rather than either SCS days or per-storm loss, implying that a shift in SCS hazard alters their indemnity relatively little. Conversely, other regions (NM, OK, TX, MS, LA, AR, WY, MT) carry a larger share in their risk in the hazard and vulnerability components. Thus, future shifts in SCS days occupy a greater portion in their risk portfolio, making them far more sensitive to physical SCS hazard changes. The present-day decomposition thus serves as a map of differential future susceptibility.

We interpret the 11% increase of total future SCS indemnity in the southern states as a first-order, physically grounded estimate rather than a calibrated forecast. This estimate is supported by two robust findings: the observed SCS day-to-loss relationship resolved across the historical records (Fig 3a; $R^2 = 0.70$) and the convection-permitting projection of the hazard itself (C404 PGW). It is also conditioned on a single forcing pathway. Although SSP3-7.0 is a high-emissions scenario

(3.6°C warming end of century) that diverges substantially from current policy trajectories under SSP2-4.5 (2.7 °C warming end of century), our 2022–2063 projection window falls entirely within the period over which these pathways have not yet separated (43). The warming level our simulation represents is therefore broadly representative of near- to mid-century conditions across plausible pathways, rather than specific to a high-emissions future.

Holding exposure and coverage fixed isolates the climate signal, making the value an intentionally conservative sensitivity unconfounded by rising liability or shifting participation. Furthermore, the sparse historical record over regions with few SCS days and limited claim history complicate future risk pricing. High-occurrence regions (NE, CO, KS, TX) operate in a domain of known unknowns: their loss distributions are well-sampled across decades of SPC reports and FCIP records, rendering extreme years legible against a stable baseline. Conversely, the sparse-record and low-coverage counties occupy a fundamentally different unknown unknown regime, in which the historical record is too sparse to estimate loss probabilities or even to characterize what an extreme SCS year looks like. Because the fitted SCS day–loss relationship has effectively no historical observational support at the higher storm frequencies projected for these regions, future loss estimate represents an extrapolation beyond the existing data. Ultimately, climate change concentrates future hazards precisely where our observational and statistical capacity is weakest, converting a localized data-sparsity problem into a systematic blind spot embedded in federal program pricing structures.

A policy logic follows from the results presented here. First, the FCIP prices SCS risk on backward-looking loss experience: county base rates are set from long historical loss-cost ratios and scaled by each farm's Actual Production History, which draws on only 4–10 years of yield records (44-45). We show that SCS hazards are expanding largely into the regions where that historical data record is thinnest, so the pricing basis is structurally weakest where it will matter most. This misalignment has a distributional consequence that runs through the coverage and subsidy mechanism: producers in Southern Great Plains and Lower Mississippi producers tend to elect lower coverage, leaving them to absorb more of each loss directly despite drawing a higher subsidy rate. As a result, the gap between priced and realized risk is ultimately borne by a combination of producers and the federal budget. The fact that the FCIP is heavily subsidized by US taxpayers means that future increase of hazards and subsequent indemnities will likely drive up the federal spending and create financial impacts far beyond the agricultural sector (35-36).

Finally, our cause-specific analysis of SCS can provide valuable insights into the feasibility of new insurance product developments (34, 36, 46). For example, area and index-based products now account for a substantial and growing share of program liability (~24% as of 2024; 47) and offer a pathway to coverage that is more accessible, more affordable, and more responsive to specific hazard profiles. This aligns with recent legislative interest, for example, the bi-partisan proposed Withstanding Extreme Agricultural Threats by Harvesting Economic Resilience Act of 2025 (WEATHER Act of 25; 48), in addressing agricultural risks from climate extremes. It also supports premium-incentivized adaptation measures, such as rewarding replanting after early-season hazards, that would make the safety net an instrument of adaptation. By synthesizing long-term

359 records from NOAA and USDA with high-resolution climate model projections, our work
360 provides the foundational hazard analysis that such products require.

Materials and Methods

In this study, we integrated datasets from multi-sector, including ground-based severe weather reports from NOAA Storm Prediction Center (SPC), a long-term (40+ years) convection-permitting (4-km) high-resolution climate downscaling in the Contiguous US (C404) for both historical (1980-2021) and future (2022-2063) climate, and USDA Federal Crop Insurance Program (FCIP).

1. NOAA SPC Severe Weather Reports

The Storm Prediction Center's (SPC) Storm Event Dataset (49) provides long-term records (since June 1, 1999) for three types of SCS: tornadoes, hail, and thunderstorm winds. These records are based on local storm reports (LSRs) from local National Weather Service (NWS) offices. Data from the 2000 to 2020 growing season (March to September) are downloaded from the SPC website: https://www.spc.noaa.gov/climo/reports/.

To facilitate comparison with county-level crop insurance data, we aggregated storm reports to county-level SCS days using Federal Information Processing Standards (FIPS) codes. The SCS day was capped at one event per day per county to avoid double-counting and mitigate population density biases, a common practice when resampling SPC data (1, 16, 23).

Two significant changes occurred during this period (2000-2020), introducing t critical discontinuities into the SPC record. First, the reporting threshold for hail increased from 0.75 to 1.0 inch at the end of 2010 (16). Second, starting in 2012, NOAA SPC implemented filtering procedures to reduce duplicate reports and limit artificially inflated estimates of severe weather events when multiple reports were submitted for the same event. These changes resulted in inconsistent trend detections: increasing trends were observed for 2000-2011 and 2012-2020 when analyzed separately, yet a decreasing trend appeared when the two periods were combined (Fig. 1d), reflecting a known artifact of the dataset. Given these data discontinuities, Fig. 1(a-c) and (e) uses the more consistent 2012-2020 period for comparison between the SPC reports and C404.

2. C404 Convection-Permitting Climate Model Data

Historical simulation. The CONUS404 (C404, 25) historical dataset is generated from a continuous regional climate simulation dynamically downscaling ERA5 reanalysis data (1980-2021) using the Weather Research and Forecasting (WRF) model. The simulation was conducted at 4-km horizontal grid spacing with 51 vertical levels. Key physics settings include the Thompson microphysics scheme, the Yonsei University planetary boundary layer scheme (YSU), the Noah-MP land surface model coupled with the MMF groundwater scheme, and RRTMG radiation schemes. Spectral nudging was applied to all state variables (except vapor mixing ratio) to constrain large-scale weather patterns to ERA5. A more detailed model description and evaluation is provided in (25), which demonstrates strong performance in capturing key meteorological fields (e.g., precipitation, temperature, snow, soil moisture, etc.) in climate research and impact studies (50-54). C404 has also reliably reproduced key climatological characteristics of mesoscale convective systems (MCSs), important drivers of SCS, across the continental US.

Future projection (PGW). The C404 future climate projection (55) simulates climate changes over 2022-2063 under the CMIP6 SSP3-7.0 scenario using the pseudo-global warming (PGW) approach, a widely adopted method in regional climate downscaling (25, 57-58). This simulation employs the same WRF model configuration as the historical run but adds a climate change signal derived from the CESM2 Large Ensemble (LENS2, 59) to the reanalysis-based forcing, enabling the future projection to capture both observed historical variability and projected climate changes, as described in Equations. (1) – (2):

$$WRF_{forcing}(t_{fut}) = ERA5(t_{hist}) + ClimSig(t_{fut}) \quad (1)$$

$$ClimSig(t_{fut}) = \overline{LENS2}(t_{fut}) - \overline{LENS2}(t_{hist}) \quad (2)$$

Computational cost and future scenario choice. Both the historical simulation and future projection, comprising two 42-year runs, were performed at 4-km grid spacing over the full CONUS on the USGS Denali system, requiring approximately 58.3 million core-hours and 15 months of wall-clock time on 62 nodes (4960 CPUs). Continental-scale convection-permitting simulations at this spatial resolution and duration approach the practical limits of current high-performance computing resources. Generating a multi-scenario or multi-GCM ensemble of comparable length is therefore computationally infeasible, as the total cost scales approximately with the number of ensemble members. These resource constraints motivated our selection of a single scenario, SSP3-7.0. Accordingly, we treat the resulting projection as a physically consistent realization of one plausible warming trajectory, rather than as an assessment of scenario uncertainty. Although SSP3-7.0 represents a high-emissions pathway, with approximately 3.6°C of end-of-century warming, that diverges substantially from current policy trajectories under SSP2-4.5, with approximately 2.7 °C of end-of-century warming), the differences in projected warming among these pathways remain comparatively modest over our 2022–2063 projection period (IPCC AR6 WG1, Table SPM.1). Consequently, the warming level represented in our simulation is broadly relevant to near- to mid-century conditions across plausible pathways, rather than being specific to a high-emissions future.

Assumptions and limitations of the PGW method. The PGW design has several important implications for interpretation. First, the perturbation is applied as a smooth, GHG-forced monthly-mean delta, such that the projected change in SCS activity is driven principally by the thermodynamic response of explicitly resolved convection to increased temperature and moisture over the CONUS. Changes in large-scale circulation, e.g. shifts in mid-latitude storm tracks, jet position, or the synoptic patterns that supply the deep-layer shear necessary to organize severe convection, are not explicitly represented, since the lateral boundary forcing retains the historical synoptic sequence. Existing projections suggest that the thermodynamic response dominates changes in severe-convective environments, with shear reductions occurring preferentially on low CAPE days f and therefore only weakly offsetting the overall CAPE increase (19); however, the observed eastward migration of tornado activity has been attributed in part to dynamical changes this framework cannot reproduce (28), and circulation change could in principle either reinforce or partially counteract the shift identified here. Second, land-surface and vegetation feedback

evolve only through the perturbed soil moisture and prescribed GHG concentrations, without accounting for changes in land cover or management.

These limitations notwithstanding, PGW remains a defensible framework for this application. Relative to more idealized approaches, such as uniform SST perturbations or radiative-equilibrium configurations, it maintains physical consistency between the perturbed thermodynamic state and explicitly resolved storm dynamics. Furthermore, retaining the observed synoptic sequence enables direct event-by-event comparisons between the historical and future integrations. The resulting projections should therefore be viewed as estimates of how SCS activity responds to thermodynamic warming and moistening under the historical sequence of large-scale circulation, rather than as a full representation of combined thermodynamic and dynamical changes. Crucially, PGW provides one of the few computationally tractable routes currently available for generating a multi-decadal convection-permitting record of severe convective activity.

3. Severe Convective Storm Proxy

Although C404 can resolve mesoscale convective systems, its 4-km grid spacing is insufficient to fully capture tornadoes and hail. Therefore, we employed a SCS proxy based on hourly composite radar reflectivity (Z) and hourly updraft helicity (UH) over the 2-5 km atmospheric layers above the ground, following previous studies (22, 26, 60). A SCS event is identified when both Z and UH exceed predefined thresholds at same grids:

$$Z >= 55 \text{ dBZ}; \text{ UH} >= 60 \text{ m/s} \quad (3)$$

Z and UH were diagnosed at model runtime, with thresholds selected to best match the NOAA SPC storm reports, at the higher end of values used in previous studies (e.g., 50 dBZ / 40 m s-1 in 22). While this proxy approach cannot distinguish between specific perils or represent microphysical hail growth, a recognized limitation, it provides a physically consistent, long-term dataset that agrees well with the spatial distribution of historical SCS hotspots and offers valuable trend information independent of observational biases (Fig. 1).

We acknowledge a key limitation in the SCS-proxy approach: the “severe” category is a generic classification that does not differentiate among specific perils like hailstorms, tornadoes, or thunderstorm winds. Our proxy does not explicitly represent the microphysical processes underlying hail formation and growth. While we observe similarities in the spatial variability of wind and hail-related insurance claims, this limitation implies that the SCS proxy is better suitable for analysis of composite severe weather threats rather than individual perils or hail size. Other studies have addressed this limitation by employing more detailed approaches, such as one-dimensional hail growth models (60) or direct graupel-size diagnostics (23) from ultra high-resolution models. Furthermore, climate change is expected to alter hailstorm characteristics, particularly hail size: while the number of hail days in summer may decrease over the Great Plains, individual storms are more likely to produce larger hail due to stronger updrafts and higher melting level heights (MLH, 28). Despite this limitation, our regional analysis of SCS remains robust and highly relevant for assessing overall SCS risk.

4. US Department of Agriculture (USDA) Federal Crop Insurance Program (FCIP)

We focused on five major US field crops (corn, soybean, wheat, rice, and cotton), which together represent most planted acreage and insured liability under the FCIP, accounting for more than 82% insured liability. Two datasets below are used to characterize exposure and vulnerability of SCS separately at the county level.

Exposure: USDA Summary of Business (SOB)

County-level total insured liability was obtained from the Risk Management Agency (RMA) Summary of Business (SOB) dataset, available from 1989 onward, to describe the degree to which agricultural production in each county is financially exposed to SCS (Fig. 2a). We also computed the coverage selection for each county-year from SOB data, and the results are shown in Fig 2c and Fig 3d-e.

Vulnerability: coverage level and per-storm loss from USDA Cause of Loss (COL)

We analyzed county-level COL data from 1989-2020 obtained from the USDA RMA. This dataset includes indemnity, premium, coverage level, and liability amounts for specific causes of loss, as reported by farmers and verified by insurance adjusters. We specifically isolated hazards related to severe convective storms: hail, tornadoes, and winds. For each individual claim, we collected the filed month, crop type, insured liability, premium, and indemnity, restricting the analysis to the primary growing season months (March through September). The combined dataset was used to calculate county-level cause-specific Loss-Cost Ratio (LCR, $C_{i,j,t}$), a unitless metric defined as the ratio of Indemnity to Liability:

$$C_{i,j,t} = (I_{i,j,t})(L_{i,t})^{-1} \qquad (4)$$

where $I_{i,j,t}$ is insurance payouts (paid indemnities) caused by crop insurance hazard *j*, relative to total liabilities $L_{i,t}$ in county *i* in year *t*. Therefore, LCR presents a direct quantitative measure of the underlying economic loss relative to the value of the assets being protected, due to specific hazard types, completely independent of the premium paid.

The LCR metric and USDA RMA data have been commonly used to assess crop production risk from natural hazards, including drought, flooding, excessive rainfall, and temperature extremes (27, 30, 32-37). This study, for the first time, quantified the crop production risk related to severe convective storms with LCR and built into the per-storm loss quantity to reflect seasonal aggregated per-storm loss due to SCS in the season.

To integrate physical hazard and financial vulnerability into a single county-level metric, we followed the crop risk framework of (6-7) with modifications suited to our multi-crop, monthly analysis. For each crop *c*, county *i*, and month *m* (March through September), we calculated the median value of (SCS indemnity / liability) × \$100 over the 32-year record (1989–2020), yielding a monthly loss-cost per \$100 of insured value:

$$V_{c,i,m} = \underset{t}{\text{median}} \left[\frac{I^{\text{SCS}}_{c,i,m,t}}{L_{c,i,m,t}} \times 100 \right], \quad t = 1989, \ldots, 2020 \tag{5}$$

where $I^{SCS}_{c,i,m,t}$ is the SCS-related indemnity and $L_{c,i,m,t}$ is the total insured liability for crop c in county i, claimed month m, and year t. On the meteorological side, we calculated the corresponding monthly SCS-day count, $H_{i,m}$, from C404 for each county over the same month. The SCS per-storm loss for a given crop and county is then:

$$R_{c,i} = \sum_{m=\text{Mar}}^{\text{Sep}} V_{c,i,m} \times H_{i,m} \tag{6}$$

The total Crop-SCS risk index per county was obtained by summing across all five crops:

$$R_i = \sum_{c=1}^{4} R_{c,i} \tag{7}$$

This index captures both the climatological frequency of SCS and the financial severity of SCS-related losses across the major US field crops (Fig. 4). Critically, because the meteorological term $H_{i,m}$ is derived from C404, the same framework can be applied under future climate conditions by substituting/surrogating the historical SCS days with that from the PGW simulation, yielding a projected per-storm loss, R_i^{PGW}. The difference between R_i^{PGW} and R_i^{CTRL} then quantifies the projected change in total SCS indemnity under climate change (Fig. 4d-e).

5. Integrated Hazard-Exposure-Vulnerability Framework

We followed the IPCC AR6 WGII's definition of climate hazard, exposure and vulnerability (IPCC AR6 WGII, 9) and other climate impact literature (8, 10). Total SCS risk is the total indemnity (I; from historical claim records). Hazard (H) refers to severe convective storm frequency (SCS days), from NOAA SPC reports and C404. Exposure (E) refers to insured liability, from USDA RMA SOB dataset. Vulnerability (V) is defined as per-storm loss and can be calculated from USDA COL claim data and historical SCS days. Total indemnity is decomposed multiplicatively:

I (total indemnity) = **H** (SCS day) x **E** (insured liability) x **V** (per-storm loss) (8)

Decomposing total risk to hazard, exposure, and vulnerability

To understand how each state is differently affected by each component, we decomposed each state's total indemnity by its deviation from the 18-state (Central US SCS Alley) mean:

$$\frac{I}{I_{\langle 18\rangle}} = \frac{H \times E \times V}{H_{\langle 18\rangle} \times E_{\langle 18\rangle} \times V_{\langle 18\rangle}} \tag{9}$$

Taking the natural log converts the multiplicative relation to an additive one:

$$\ln I - \ln I_{\langle 18\rangle} = \left(\ln H - \ln H_{\langle 18\rangle}\right) + \left(\ln E - \ln E_{\langle 18\rangle}\right) + \left(\ln V - \ln V_{\langle 18\rangle}\right)$$

$$\Delta \ln I = \Delta \ln H + \Delta \ln E + \Delta \ln V \tag{10}$$

We applied this to the top 18 most-impacted states in the central-US SCS Alley (Fig. 3c). Ranking from top to bottom, we analyzed which components contribute positively or negatively to a state being above or below the 18-state average in a bar plot (Fig. 3c).

Data Availability

All data used in this analysis are publicly available for purposes of reproducing or extending the analysis. The datasets can be accessed through the following repositories and databases:

- WRF CONUS404: The high-resolution regional climate simulation data are available through the National Center for Atmospheric Research (NCAR) Geoscience Data Exchange (GDEX) platform at https://gdex.ucar.edu/datasets/d559000/
- Severe Weather Reports: The severe convective storm report data are provided by the National Oceanic and Atmospheric Administration (NOAA) Storm Prediction Center (SPC) and can be accessed at https://www.spc.noaa.gov/climo/reports/.
- Crop Insurance Data: The Federal Crop Insurance Corporation (FCIP) data are publicly available from the USDA Risk Management Agency (RMA). The Summary of Business records: https://www.rma.usda.gov/tools-reports/summary-of-business, and the Cause of Loss records: https://www.rma.usda.gov/tools-reports/summary-of-business/cause-loss.

References

(1) Prein, A. F., Holland, G. J. (2018). Global estimates of damaging hail hazard. Weather and Climate Extremes, Volume 22, 2018, Pages 10-23, https://doi.org/10.1016/j.wace.2018.10.004.

(2) Changnon, S. A. (2009). Increasing major hail losses in the U.S. 10.1007/s10584-009-9597-z

(3) Changnon, S. A., Stout, G. E. (1966). Crop-Hail Intensities in Central and Northwest United States.10.1175/1520-0450(1967)006<0542:CHIICA>2.0.CO;2

(4) Changnon, S. A. (1971) Hailfall Characteristics Related to Crop Damage

10.1175/1520-0450(1971)010<0270:HCRTCD>2.0.CO;2

(5) Changnon, S. A. (1972). Examples of Economic Losses from Hail in the United States

(6) Changnon, D., Changnon, S. A. (1997) Surrogate Data to Estimate Crop-Hail Loss. 10.1175/1520-0450(1997)036<1202:SDTECH>2.0.CO;2

(7) Changnon, S. A. (1999) Data and Approaches for Determining Hail Risk in the Contiguous United States. 10.1175/1520-0450(1999)038<1730:DAAFDH>2.0.CO;2

(8) Bouwer, L.M. (2019). Observed and Projected Impacts from Extreme Weather Events: Implications for Loss and Damage. In: Mechler, R., Bouwer, L., Schinko, T., Surminski, S., Linnerooth-Bayer, J. (eds) Loss and Damage from Climate Change. Climate Risk Management, Policy and Governance. Springer, Cham. https://doi.org/10.1007/978-3-319-72026-5_3

(9) IPCC, 2022: Summary for Policymakers [H.-O. Pörtner, D.C. Roberts, E.S. Poloczanska, K. Mintenbeck, M. Tignor, A. Alegría, M. Craig, S. Langsdorf, S. Löschke, V. Möller, A. Okem (eds.)]. In: Climate Change 2022: Impacts, Adaptation and Vulnerability. Contribution of Working Group II to the Sixth Assessment Report of the Intergovernmental Panel on Climate Change [H.-O. Pörtner, D.C. Roberts, M. Tignor, E.S. Poloczanska, K. Mintenbeck, A. Alegría, M. Craig, S. Langsdorf, S. Löschke, V. Möller, A. Okem, B. Rama (eds.)]. Cambridge University Press, Cambridge, UK and New York, NY, USA, pp. 3–33, doi:10.1017/9781009325844.001.

(10) Viner D, Ekstrom M, Hulbert M, Warner NK, Wreford A, Zommers Z. Understanding the dynamic nature of risk in climate change assessments—A new starting point for discussion. Atmos Sci Lett. 2020;21:e958. https://doi-org.cuucar.idm.oclc.org/10.1002/asl.958

(11) Childs, Russ, Demuth. Agricultural Perspectives on Hailstorm Severity, Vulnerability, and Risk Messaging in Eastern Colorado.10.1175/WCAS-D-20-0015.1

(12) Changnon, S. A., Changnon, D. (2000). Long-Term Fluctuations in Hail Incidences in the United States. 10.1175/1520-0442(2000)013<0658:LTFIHI>2.0.CO;2

(13) Raupach, T. H., Martius, O., Allen, J. T., Kunz, M., Trapp, S. L.-, Mohr, S., Rasmussen, K. L., & Trapp, R. J. (2021). The effects of climate change on hailstorms. Nature Reviews Earth & Environment, 2(March). https://doi.org/10.1038/s43017-020-00133-9.

(14) Raupach, T.H., Portmann, R., Siderius, C. et al. Shifting hail hazard under global warming and effects on crop hail risk. Nat. Clim. Chang. 16, 696–703 (2026). https://doi-org.cuucar.idm.oclc.org/10.1038/s41558-026-02660-7

(15) Zhang, S., Zhang, Q., Allen, J.T. et al. Rising global hail damage potential in a warming world. Nature 653, 1069–1077 (2026).

(16) Allen, J. T., & Tippett, M. K. (2015). The Characteristics of United States Hail Reports : 1955 – 2014. 10(3), 1–31. Electron. J. Severe Storms Meteor., 10 (3), https://www.ejssm.org/ojs/index.php/ejssm/article/viewArticle/149.

(17) Taszarek, M., Allen, J., Groenemeijer, P., Edwards, R., Brooks, H., Chmielewski, V., Enno, S-E. (2020). Severe Convective Storms across Europe and the United States. Part I: Climatology of Lightning, Large Hail, Severe Wind, and Tornadoes. 10239–10261. https://doi.org/10.1175/JCLI-D-20-0345.1

(18) Trapp, R. J., Diffenbaugh, N. S., Brooks, H. E., Baldwin, M. E., Robinson, E. D., & Pal, J. S. (2007). Changes in severe thunderstorm environment frequency during the 21st century caused by anthropogenically enhanced global radiative forcing. https://doi.org/10.1073/pnas.0705494104

(19) Diffenbaugh, N. S., Scherer, M., & Trapp, R. J. (2013). Robust increases in severe thunderstorm environments in response to greenhouse forcing. 110(41). https://doi.org/10.1073/pnas.1307758110

(20) Prein, A. F., Langhans, W., Fosser, G., Ferrone, A., Ban, N., Goergen, K., Keller, M., Tölle, M., Gutjahr, O., Feser, F., Brisson, E., Kollet, S., Schmidli, J., Van Lipzig, N. P. M., & Leung, R. (2015). A review on regional convection-permitting climate modeling: Demonstrations, prospects, and challenges. Reviews of Geophysics, 53(2), 323–361. https://doi.org/10.1002/2014RG000475

(21) Lucas-Picher, P., Argüeso, D., Brisson, E., Tramblay, Y., Berg, P., Lemonsu, A., Kotlarski, S., & Caillaud, C. (2021). Convection-permitting modeling with regional climate models: Latest developments and next steps. Wiley Interdisciplinary Reviews: Climate Change, 12(6), e731. https://doi.org/10.1002/wcc.731

(22) Trapp, R. J., Robinson, E. D., Baldwin, M. E., Diffenbaugh, N. S., & Schwedler, B. R. J. (2011). Regional climate of hazardous convective weather through high-resolution dynamical downscaling. 677–688. https://doi.org/10.1007/s00382-010-0826-y

(23) Trapp, R. J., Hoogewind, K. A., & Lasher-Trapp, S. (2019). Future Changes in Hail Occurrence in the United States Determined through Convection-Permitting Dynamical Downscaling. 2018, 5493–5509. https://doi.org/10.1175/JCLI-D-18-0740.1

(24) Prein, A., Liu, C., Ikeda, K., Bullock, R., Rasmussen, R., Holland, G., & Clark, M. (2020). Simulating North American mesoscale convective systems with a convection-permitting climate model. Climate Dynamics, 55, 95–110. https://doi.org/10.1007/s00382-017-3993-2

(25) Rasmussen, R. M., Chen, F., Liu, C. H., Ikeda, K., Prein, A., Kim, J., Schneider, T., Dai, A., Gochis, D., Dugger, A., Zhang, Y., Jaye, A., Dudhia, J., He, C., Harrold, M., Xue, L., Chen, S., Newman, A., Dougherty, E., … Miguez-Macho, G. (2023). CONUS404: The NCAR-USGS 4-km long-term regional hydroclimate reanalysis over the CONUS. Bulletin of the American Meteorological Society. https://doi.org/10.1175/BAMS-D-21-0326.1

(26) Liu, C., Ikeda, K., & Rasmussen, R. (2024). Severe Convective Weather in the Central and Eastern United States : Present and Future. Atmosphere 2024, 15(12), 1444; https://doi.org/10.3390/atmos15121444

(27) Gensini, V. A., & Mote, T. L. (2014). Estimations of Hazardous Convective Weather in the United States Using Dynamical Downscaling. 6581–6589. https://doi.org/10.1175/JCLI-D-13-00777.1

(28) Gensini, V.A., Brooks, H.E. Spatial trends in United States tornado frequency. npj Clim Atmos Sci 1, 38 (2018). https://doi-org.cuucar.idm.oclc.org/10.1038/s41612-018-0048-2

(29) Hoogewind, K. A., Baldwin, M. E., & Trapp, R. J. (2017). The Impact of Climate Change on Hazardous Convective Weather in the United States : Insight from High-Resolution Dynamical Downscaling. 10081–10100. https://doi.org/10.1175/JCLI-D-16-0885.1

(30) Bundy, Gensini, Russo et al., 2022. Insured Corn Losses in the United States from Weather and Climate Peril. https://doi.org/10.1175/JAMC-D-21-0245.1

(31) Battaglioli, F., Taszarek, M., Groenemeijer, P. et al. Contrasting trends in very large hail events and related economic losses across the globe. Nat. Geosci. 19, 52–58 (2026).

(32) Li, Y., Guan, K., Schnitkey, G. D., Delucia, E., & Peng, B. (2019). Excessive rainfall leads to maize yield loss of a comparable magnitude to extreme drought in the United States. October 2018, 2325–2337. https://doi.org/10.1111/gcb.14628

(33) Reyes, J. J., & Elias, E. (2019). Spatio-temporal variation of crop loss in the United States from 2001 to 2016

(34) Perry, E. D., & Yu, J. (2020). Using insurance data to quantify the multidimensional impacts of warming temperatures on yield risk. Nature Communications, 2020, 1–9. https://doi.org/10.1038/s41467-020-17707-2

(35) Noah S Diffenbaugh et al (2021). Historical warming has increased U.S. crop insurance losses. Environ. Res. Lett. 16 084025, DOI 10.1088/1748-9326/ac1223

(36) Benami, E., Jin, Z., Carter, M.R. et al. Uniting remote sensing, crop modelling and economics for agricultural risk management. Nat Rev Earth Environ 2, 140–159 (2021). https://doi.org/10.1038/s43017-020-00122-y

(37) Choi, E., Rigden, A. J., Tangdamrongsub, N., Jasinski, M. F., & Mueller, N. D. (2024). US crop yield losses from hydroclimatic hazards. Environmental Research Letters, 19(1), 14005. https://doi.org/10.1088/1748-9326/ad0c87

(38) O'Donoghue, Erik J. The Effects of Premium Subsidies on Demand for Crop Insurance, ERR-169, U.S. Department of Agriculture, Economic Research Service, July 2014.

(39) Coble, K.H. and Barnett, B.J. (2013), Why Do We Subsidize Crop Insurance? Amer. J of Ag. Econ., 95: 498-504.

(40) Yi, J., Bryant, H.L. & Richardson, J.W. How do premium subsidies affect crop insurance demand at different coverage levels: the case of corn. Geneva Pap Risk Insur Issues Pract 45, 5–28 (2020).

(41) The 1996 U.S. Farm Act Increases Market Orientation. By C. Edwin Young and Paul C. Westcott, Commercial Agriculture Division, Economic Research Service, U.S. Department of Agriculture, Agriculture Information Bulletin No. 726.

(42) Carroll-Smith, Dereka and Done, James and Prein, Andreas F. and Aldridge, Joanna and Ge, Ming, Historical and Future U.S. Large Hail Frequency using Ensemble Climate Simulation. Available at SSRN: https://ssrn.com/abstract=6569202 or http://dx.doi.org/10.2139/ssrn.6569202

(43) IPCC, 2021: Summary for Policymakers. In: Climate Change 2021: The Physical Science Basis. Contribution of Working Group I to the Sixth Assessment Report of the Intergovernmental Panel on Climate Change [Masson-Delmotte, V., P. Zhai, A. Pirani, S.L. Connors, C. Péan, S. Berger, N. Caud, Y. Chen, L. Goldfarb, M.I. Gomis, M. Huang, K. Leitzell, E. Lonnoy, J.B.R. Matthews, T.K. Maycock, T. Waterfield, O. Yelekçi, R. Yu, and B. Zhou (eds.)]. Cambridge University Press, Cambridge, United Kingdom and New York, NY, USA, pp. 3−32, doi:10.1017/9781009157896.001.

(44) Liu, Yong, and A. Ford Ramsey. 2023. "Incorporating Historical Weather Information in Crop Insurance Rating." American Journal of Agricultural Economics 105(2): 546–575. https://doi.org/10.1111/ajae.12329

(45) Coble, K.H., T.O. Knight, B.K. Goodwin, M.F. Miller, and R.M. Rejesus. 2010. A Comprehensive Review of the RMA APH and COMBO Rating Methodology: Final Report. Prepared by Sumaria Systems for the USDA Risk Management Agency.

(46) Brown, M., Osgood, D. & Carriquiry, M. Science-based insurance. Nature Geosci 4, 213–214 (2011). https://doi.org/10.1038/ngeo1117

(47) Source: USDA, Economic Research Service, using data from USDA, Risk Management Agency

(48) S.231 - 119th Congress (2025-2026): WEATHER Act of 2025. (2025, January 23). https://www.congress.gov/bill/119th-congress/senate-bill/231

(49) Schaefer, J., Levit, J., Weiss, S., and McCarthy, D. (2004) The frequency of large hail over the contiguous United States. 14th Conference on Applied Climatology.

(50) Prein, A. F. (2023). Thunderstorm straight line winds intensify with climate change. Nature Climate Change, 13(12), 1353–1359. https://doi.org/10.1038/s41558-023-01852-9

(51) Abolafia-Rosenzweig, R., He, C., Chen, F., Ikeda, K., Schneider, T., & Rasmussen, R. (2023). High resolution forecasting of summer drought in the western United States. Water Resources Research, 59, e2022WR033734. https:// doi.org/10.1029/2022WR033734

(52) Qin, H., Alvee, F. M., Leung, L. R., Sun, X., & Wang, G. (2025). Performance of Convection-Permitting and Convection-Parameterized Models in Reproducing the Extreme Precipitation Intensity Relationship with Surface Conditions. Journal of Climate, 4611–4623, https://doi.org/10.1175/JCLI-D-24-0589.1

(53) Nerantzaki, S. D., Abdelmoaty, H. M., Papalexiou, S. M., & Newman, A. J. (2025). The influence of atmospheric drivers, environmental factors, and urban land use on extreme hourly precipitation trends over the CONtiguous United States for 40 years at 4-km resolution (CONUS404). Science of the Total Environment, 969, 178407.

(54) Dougherty, E., Tessendorf, S., & DeCastro, A. (2025). Historical Warming and Drying in Colorado and Their Impact on Cool-Season Precipitation and Snow. 1261–1273. https://doi.org/10.1175/JHM-D-24-0153.1

(55) Xue, L., Rasmussen, R.M., Chen, F., Liu, C., Ikeda, K., Prein, A., Kim, J., Schneider, T.L., Dai, A., Gochis, D., Dugger, A., Zhang, Y., Jaye, A., Dudhia, J., He, C., Harrold, M., Chen, S., Newman, A., Dougherty, E., Abolafia-Rozenzweig, R., Lybarger, N., Viger, R., Rasmussen, K., and Miguez-Macho, G., 2024, CONUS404 PGW: Four-kilometer long-term regional hydroclimate reanalysis perturbed with pseudo-global warming (PGW) conditions over the conterminous United States: U.S. Geological Survey data release, https://doi.org/10.5066/P9HH85UU.

(56) Schär, C., Frei, C., Lüthi, D., & Davies, H. C. (1996). Surrogate climate-change scenarios for regional climate models. *Geophysical Research Letters*, *23*(6), 669–672. https://doi.org/10.1029/96GL00265

(57) Rasmussen, R., Liu, C., Ikeda, K., Gochis, D., Yates, D., Chen, F., Tewari, M., Barlage, M., Dudhia, J., Yu, W., Miller, K., Arsenault, K., Grubišić, V., Thompson, G., & Gutmann, E. (2011). High-resolution coupled climate runoff simulations of seasonal snowfall over Colorado: A process study of current and warmer climate. *Journal of Climate*, *24*(12), 3015–3048. https://doi.org/10.1175/2010JCLI3985.

(58) Liu, C., Ikeda, K., Rasmussen, R., Barlage, M., Newman, A. J., Prein, A. F., Chen, F., Chen, L., Clark, M., Dai, A., Dudhia, J., Eidhammer, T., Gochis, D., Gutmann, E., Kurkute, S., Li, Y., Thompson, G., & Yates, D. (2017). Continental-scale convection-permitting modeling of the current and future climate of North America. *Climate Dynamics*, *49*(1–2), 71–95.

(59) Rodgers, K. B., Lee, S., Rosenbloom, N., Timmermann, A., Danabasoglu, G., Yamaguchi, R., Bódai, T., Chung, E., Huang, L., & Kim, W. M. (2021). Ubiquity of human-induced changes in climate variability. 1393–1411.1

(60) Brimelow, J., Burrows, W. & Hanesiak, J. The changing hail threat over North America in response to anthropogenic climate change. Nature Clim Change 7, 516–522 (2017).

Acknowledgements

This study was funded by the NSF National Center for Atmospheric Research (NCAR)'s Advanced Study Program Postdoctoral Fellowship, NCAR's Water Systems Program, NSF Convergence Accelerator Program Track J Phase 2 Award #2345039, NASA LCLUC Grant #80NSSC25K7490, and US Geological Survey (USGS) Water Mission Area's Integrated Water Prediction Program (Grant #140G0121F0357). This material is based upon work supported by the NSF NCAR, which is a major facility sponsored by the NSF under Cooperative Agreement No. 1852977. We would like to acknowledge high-performance computing support from Derecho provided by NCAR's Computational and Information Systems Laboratory, sponsored by the NSF, and the USGS Denali Supercomputer. Any opinions, findings, conclusions, or recommendations expressed in this publication are those of the authors and do not necessarily reflect the views of the federal government agencies.

Ethics declarations

Competing interests

Authors declare that they have no competing interests.

Supplementary Information

Supplementary Information: All supplementary figures and texts are provided in a separated PDF file included in the submission.

Materials and Methods

Figs. S1 to S11

Tables S1

Supplementary Files

This is a list of supplementary files associated with this preprint. Click to download.

- C404cropinsurancesupplementary.pdf